# ATMOSPHERIC ROTORS:
## AIRCRAFT IN SITU AND CLOUD RADAR MEASUREMENTS IN T-REX

Vanda Grubišić,[1] Larry Armi,[2] Joachim Kuettner,[3]
Samuel Haimov,[4] Larry Oolman,[4] Rick Damiani,[4]
and Brian Billings[1]

[1] Desert Research Institute, Reno, NV
[2] Scripps Institution of Oceanography, La Jolla, CA
[3] NCAR, Boulder, CO
[4] University of Wyoming, Laramie, WY

## 1. INTRODUCTION

During the Terrain-induced Rotor Experiment (T-REX; Grubišić et al. 2004) in March and April 2006, highly turbulent flows in atmospheric rotors in the lee of the Sierra Nevada were probed by the University of Wyoming King Air (UWKA) aircraft. *In situ* thermodynamic and kinematic data was obtained on rotor circulations and wave structures over Owens Valley in a number of research missions under strong wave and rotor conditions (Grubišić and Doyle 2006). Sufficiently strong signal returns from the Wyoming Cloud Radar (WCR) on board UWKA were granted by the presence of ice particles within different types of clouds associated with the wave/rotor system, including mountain cap clouds over the Sierra crest, "spill over" clouds over the eastern Sierra slopes as well as wave and rotor clouds over Owens Valley. In this study, we analyze the observed waves and rotors using primarily UWKA and WCR data. High-resolution real-data COAMPS simulations are used to provide further insight into the overall evolution and structure of airflow over the Sierra Nevada and Owens Valley. The particular focus of this paper is on Intensive Observed Period (IOP) 11 that was conducted on April 9, 2006.
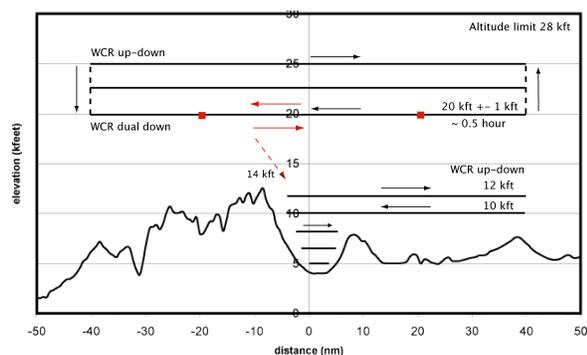


FIG. 1: T-REX UWKA flight-plan schematic with generic cross-mountain flight tracks over the Sierra Nevada and Inyo ranges. Red squares indicate end points of shorter cross-mountain tracks used in a number of research missions, including IOP 11. Gap between the upper and lower set of tracks was necessary to avoid rotor clouds given the Visual Flight Rules (VFR) within the used airspace.
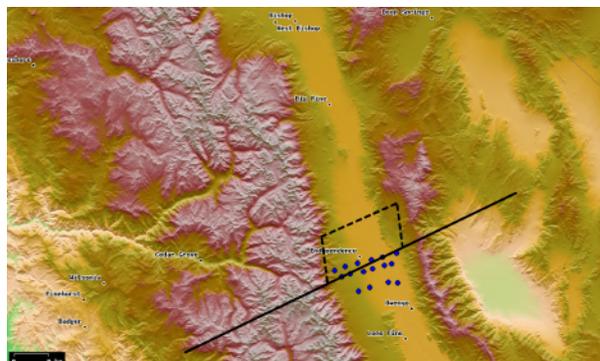


FIG. 2: T-REX UWKA flight-plan schematic showing basic Track B option. Dashed lines indicate a horizontal box pattern that was flown within the valley in a number of UWKA T-REX missions. Blue circles indicate locations of the DRI automatic weather stations.

## 2. KING AIR RESEARCH MISSIONS IN T-REX

Of the three T-REX aircraft, the UWKA flew closest to rotors, documenting the flow structure and evolution above and below the Sierra Nevada crest and penetrating a number of rotors. The basic UWKA flight pattern in T-REX consisted of a cross-mountain track flown at a number of altitudes above the Sierra crest, and a series of short, densely spaced legs within Owens Valley (Fig. 1). Instead of a dense vertical stack, a box pattern at a (smaller) number of different altitudes was flown within Owens Valley in a number of missions to examine also the along-valley variation of the low-level flow field (Fig. 2). There were three basic orientations of cross-mountain tracks: Track A (275 deg), Track B (245 deg), and Track C (215 deg).

## 3. IOP 11

Intensive Observing Period (IOP) 11 was conducted from 2200 UTC April 9 to 0200 UTC April 10 to capture a forecasted short-lived strong westerly wind event in Owens Valley associated with the passage of a transient shortwave through a larger-scale trough located upwind of the Sierra Nevada.

The UWKA flew a four hour research mission during this IOP. A vertically stacked pattern along Track B was flown at a series of altitudes, from 7,600 m MSL above
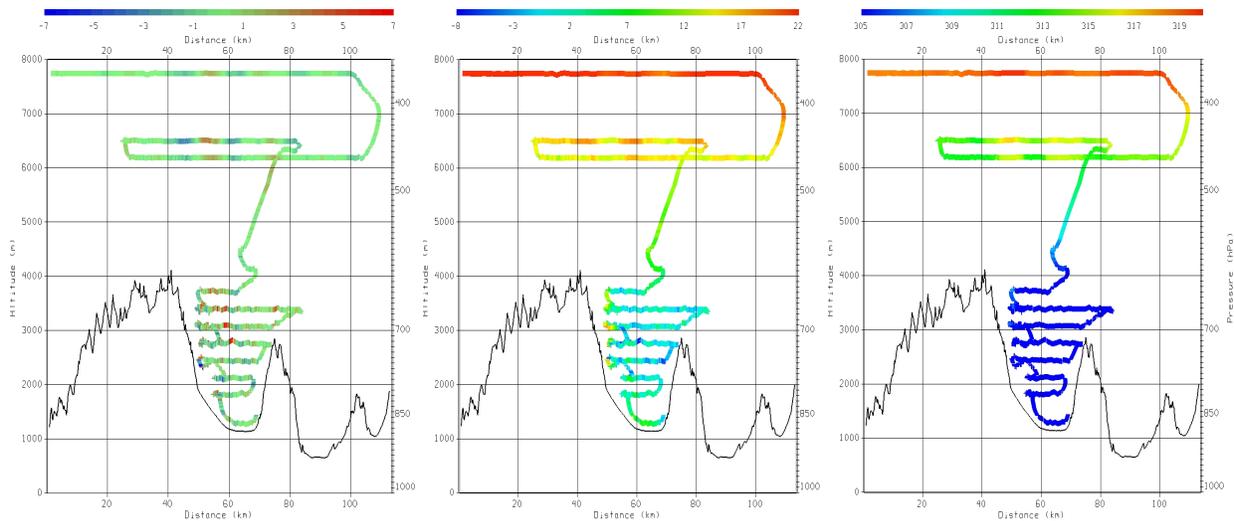
FIG. 4: IOP 11 UWKA *in situ* data from 222300 UTC April 9 to 002800 UTC April 10 displayed along the aircraft flight track. Left: Vertical velocity (m s$^{-1}$). Middle: E-W component of horizontal wind (m s$^{-1}$; positive is to the east). Right: Potential temperature (K).



FIG. 3: The Sierra cap cloud and rotor cloud over Owens Valley as seen from the ground at 2311 UTC April 9. The view is toward NNW from west of Lone Pine, CA. The photo site is located approximately 15 km to the south of the UWKA track. Photo obtained as part of the DRI/MDML photogrammetric project.

the mountains and Owens Valley to 150 m above the valley floor. The stack increment was 300 m within Owens Valley, below the base of the rotor cloud. One full stack was completed during this mission. The stacked pattern was similar to that shown in Fig. 1 due to the presence of a substantial rotor cloud (Fig. 3). Immediately upon completion of that stack, an attempt was made to repeat the entire pattern. The second stack was only partially completed due to lack of time, and was limited to four legs above the Sierra (three legs between 6,000 and 8,000 m and a leg at ~4,500 m) plus one short leg below the Sierra crest.

### 3.1 *Aircraft In Situ Data*

Figure 4 shows the vertical velocity, eastern component of horizontal velocity, and potential temperature from the first vertical stack, revealing a well defined wave

pattern with the horizontal wavelength close to 20 km downwind of the Sierra Nevada. This pattern is clearly evident at the three highest altitudes flown, with the largest amplitude at 6,300 m MSL. The first dowdraft-updraft pair in the lee of the Sierra was the strongest with amplitude of (-3.3, +3.9) m s$^{-1}$ at this altitude (cf. Fig. 5). In contrast to a relatively smooth wave pattern at these altitudes, the air encountered at lower altitudes within the valley was very turbulent. Strongest updrafts were encountered over the center of Owens Valley at altitudes between 2,500 and 3,500 m MSL (max close to 9 m s$^{-1}$). A strong downdraft was captured close to the Sierra slopes, at the western end of one of the short legs, some of which penetrated into the shooting downslope flow in the Sierra lee. Potential temperature shows a deep layer of well-mixed atmosphere within the valley reaching almost to 4 km MSL, in good agreement with the temperature profile from the GPS radiosonde released at 2306 UTC from Independence in Owens Valley (not shown). This same sounding shows also S-SE winds within the well-mixed layer in the valley, whereas the aircraft measured wind at the two lowest altitudes above the valley floor is clearly westerly. This discrepancy comes from the rapidly changing nature of the flow and the time difference between the start time of the sounding and the end time of the aircraft vertical stack ($\Delta t \approx 1.5$ hrs). This unsteadiness needs to be taken into account when interpreting the aircraft *in situ* measurements within the valley.

Comparing the vertical velocity measured at altitudes between 6,000 and 8,000 m MSL in the first and the second stack (Fig. 5), it is clear that the wave structure at these altitudes had changed less dramatically within two hours than the flow at low altitudes within the valley. Nevertheless, in between the first and the second pass at these altitudes, the first updraft in the Sierra lee had become narrower, had shifted slightly upstream, and had increased in strength to the maximum of 5.2 m s$^{-1}$. The strongest (fairly narrow) downdraft (-4.3 m s$^{-1}$)
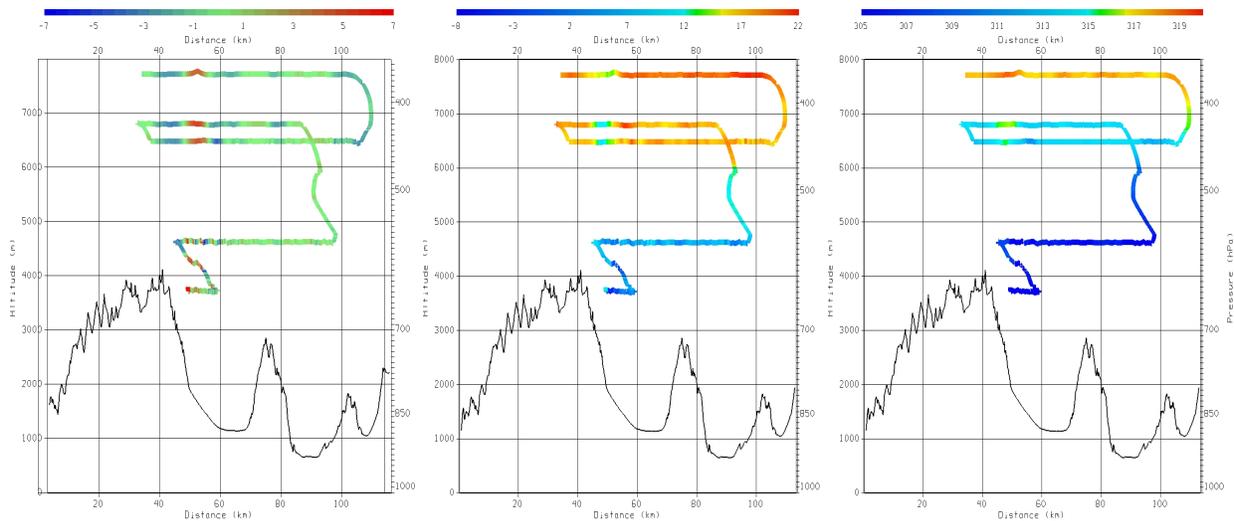
FIG. 6: As in Fig. 4 but for 0044 UTC to 0136 UTC April 10.
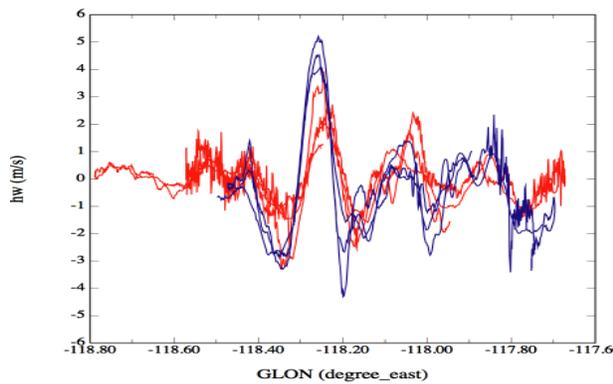


FIG. 5: UWKA measured vertical velocity (m s$^{-1}$) between 6,000 and 8,000 m MSL from 222330 UTC to 231200 UTC April 9 (red) and from 004330 to 011600 UTC April 10 (blue). The Sierra Nevada and the Inyo ridge lines are located, respectively, near -118.35° and -118.0°.

was encountered to the east of the leading edge updraft. While the amplitude of the leading updraft had increased, the amplitude of the second wave downwind had decreased. The horizontal wind perturbation associated with the leading updraft had also increased in strength, becoming clearly identifiable at all three altitudes between 6,000 and 8,000 m within the second stack (Fig. 6). The 4,500 m leg of the second stack reaches only slightly to the east of the Sierra crest; sufficiently far west, however, to show the contrast between the smooth downdraft in the Sierra lee and a highly turbulent flow just to the east of it. The downslope flow has slightly higher potential temperature than the adjoining air at the same altitude over the valley, indicating a strong downward deflection of isentropes in the immediate lee of the Sierra.

### 3.2 *WCR Data*

Good radar returns obtained in IOP 11 allowed dual-Doppler analyses (Damiani and Haimov 2006) of air motions both over the Sierra Nevada as well as over Owens Valley. Figure 7 shows such an analysis for the time segment 230535 to 231140 UTC April 9, obtained while the aircraft was flying at approximately 6,300 m MSL, heading eastward from the Sierra Nevada towards the Inyo range. Over the Sierra, a thick cap cloud reaches all the way from the ground to the flight level. Over Owens Valley there is a substantial rotor cloud with the base around 4 km and tops reaching flight level. Immediately east of the Sierra crest, there is a "spill-over" cloud with a slanted top indicating cloud evaporation due to the downward air motion in the Sierra lee. The gap between the eastern tip of this cloud and the rotor cloud over Owens Valley is the evidence of a Foehn gap. Two subsets of this dual Doppler analysis are highlighted in the insets in Fig. 7, revealing a wealth of small-scale structures in both the cap cloud as well as the rotor cloud.

The radar analysis of the rotor cloud reveals a ragged, almost vertical, western edge, a much smoother and elongated eastern end, a broad convex shape, and a two-layer structure to this cloud. Most of these features appear consistent with the image of the rotor cloud obtained from the ground (Fig. 3), and the aircraft *in situ* data. The analysis of flow within the cap cloud indicates presence of flow perturbations in the lee of individual Sierra peaks. A more detailed view of those flow structures was afforded by an earlier data segment obtained from 6,000 m MSL (Fig. 8), which preceded the one shown in Fig. 7. In the right panel of Fig. 8, horizontal lee vortices, resulting from the boundary-layer separation from the individual peaks are clearly visible; the type of lee side-vortices that are quite common in the laboratory and ocean flows (Farmer and Armi 1999). The analysis of the underlying terrain has shown that these three peaks are actually a series of short N-S ridges within the Sierra
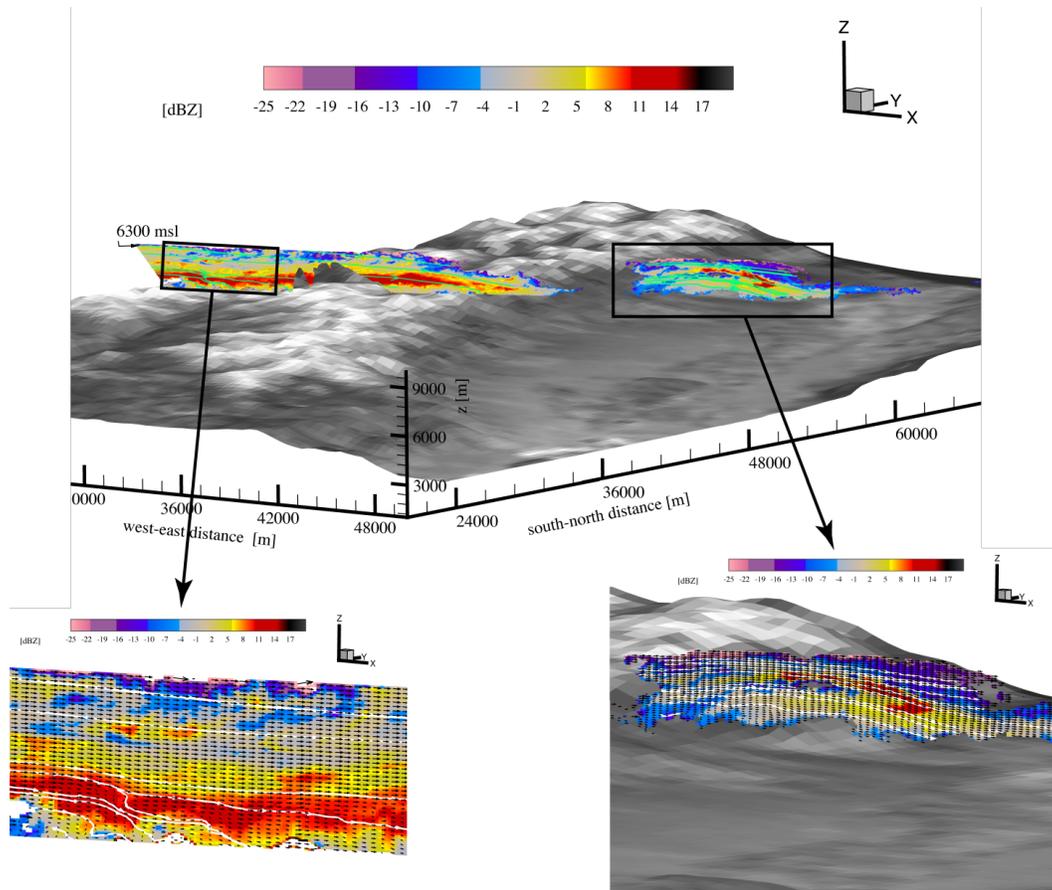
FIG. 7: Top: Dual-Doppler analysis of WCR data obtained from 230535 UTC to 231140 UTC April 9 along the cross-mountain flight track flown at approximately 6,300 m. The 2D radar segment is shown in a 3D perspective plot with the Sierra Nevada and Owens Valley terrain. Radar reflectivity (dBz in color) and streamlines (green lines). The segment of data over the Sierra had to be removed because of the aircraft's adjustment of heading. Solid boxes enclose data segments shown in the two insets. Insets: Reflectivity (dBz in color), wind (black vectors) and streamlines (white lines) from the segment of the cap cloud over the Sierra Nevada and the rotor cloud over Owens Valley.

crest. Thus, this dual-Doppler radar analysis appears to present evidence of boundary layer separation at a salient edge (Prandtl 1952; Batchelor 1967) occurring in the atmosphere.

### 3.3 Numerical Simulations

High-resolution numerical simulations (333 m finest grid increment) were performed using the atmospheric module of the Naval Research Laboratory's Coupled Ocean/Atmosphere Mesoscale Prediction System (COAMPS$^{TM}$). The model setup is identical to that used in Grubišić and Billings (2006). Five nested domains, sixty unevenly distributed vertical sigma levels with finer spacing near the ground, and a full set of physical parameterizations were used in this simulation. Lateral boundary conditions were specified using the Navy's global model (NOGAPS) forecast fields, while the initial conditions were created by blending the previous 12-hr COAMPS ("cold-start") forecast with the NOGAPS analysis and assimilated synoptic observations.

The IOP 11 simulation was performed for the period 1300 UTC March 9 to 1200 UTC March 10. The verification of the simulation results with surface wind measurements from the DRI surface stations shows that there is approximately two-hour delay in the model timing of the low-level flow development as evidenced by the westerly momentum penetration to the ground into the valley. This delay could be related to the large-scale synoptic flow conditions, particularly the timing of the shortwave passage upstream of the Sierra crest that creates the needed temperature difference between the air upstream of the Sierra Nevada and that over Owens Valley as well as the change of the upstream wind direction from SSW to a more optimal SW direction. With this caveat in mind, in Fig. 9 we show the model predictions in a vertical cross-section whose base is along the UWKA flight track. Assuming a time delay of two hours, the shown model snapshots correspond, from left to right, to: i) beginning of the first stack (~2300 UTC Apr 9), ii) beginning of the second stack (~0100 UTC Apr 10) and iii) the end of the research
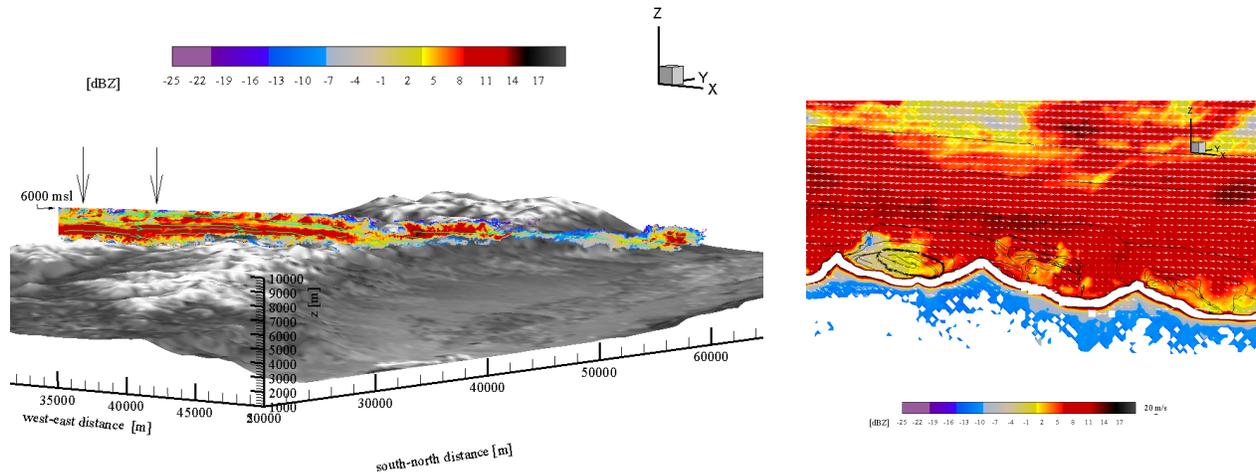
FIG. 8: Left: As in Fig. 7 but for the data segment from 225455 UTC to 230220 UTC April 9 obtained along the cross-mountain flight track flown at ~6,000 m. The pair of vertical arrows indicate the start and end points of the data segment shown to the right. Right: Zoom of the dual-Doppler analysis within the cap cloud over the Sierra Nevada showing horizontal lee vortices in the wake of short N-S oriented ridges within the Sierra ridge. Radar reflectivity (dBz in color), wind (white vectors), and streamlines (black lines). Thick white line represents the outline of the underlying terrain.

mission (~0200 UTC Apr 10).

At the first model output time shown in Fig. 9 we see the beginning of downslope flow penetration into the valley that has started to displace the strong SE flow still present within the valley at this time. At one hour preceding this time, the model solution shows moderate waves in SSW flow above the Sierra crest decoupled from the strong SE flow within the well-mixed air in the valley (not shown). The shooting downslope flow gradually undercuts and ultimately displaces the SE flow within the valley. The model solution indicates that this downslope flow is part of a large-amplitude strongly non-linear flow response within the valley that resembles an internal hydraulic jump. The wave-induced (or "jump-induced") reversed pressure gradient leads to the significant deceleration of the flow underneath the jump at the ground and eventually to the wave-induced boundary layer separation and the appearance of the reversed flow at the ground (Baines 1995; Doyle and Durran 2002; Grubišić and Billings 2006). While this separation is clearly evident in these cross sections only in the lee of the Inyo range, the model predicts the reversed flow at the ground also in the lee of the Sierra at locations slightly to the north of the shown cross-section.

## 4. DISCUSSION AND FUTURE WORK

The presented composite analysis of the *in situ* aircraft data and the dual-Doppler radar data shows a rapidly evolving wave and rotor event. The *in situ* aircraft data shows a series of moderate amplitude waves transitioning into one dominant downdraft-updraft couplet in the lee of the Sierra at altitudes above 6,000 m MSL, and reveals the contrast between the smooth downslope flow over the Sierra lee slopes and turbulent flow over Owens Valley near and below the Sierra crest. The dual-Doppler analyses of air motions within the cap cloud, the spill-over

cloud and the rotor cloud provide the information on airflow structure within these clouds and reveal the wealth of small-scale structures both within the rotor cloud and the cap cloud. Within the latter, the dual-Doppler analysis shows presence of smaller-scale horizontal lee-vortices in the lee of individual short and steep ridges within the Sierra crest.

The high-resolution COAMPS simulation provides a wider context for this rapidly evolving wave/rotor event. The model results show the transition from a flow state with moderate-amplitude waves above the Sierra crest that are decoupled from a strong SE flow within the valley to a highly non-linear flow state with a turbulent rotor above Owens Valley. This rotor appears to be associated with an internal hydraulic jump in the lee of the Sierra Nevada (Kuettner 1959). The jump is accompanied by a low-level wave breaking over the Sierra lee slopes and shooting downslope flow underneath the wave breaking zone. The high-resolution model simulation results indicate that the wave- (or jump-)induced adverse pressure gradient ultimately leads to the boundary layer separation and the appearance of the reversed flow at the ground underneath the jump.

Future work will include several other T-REX IOPs with strong rotors, including IOP 3 (Mar 9–10), IOP 4 (Mar 13–14), IOP 6 (Mar 24–25), and IOP 13 (Apr 15–16). Good radar returns are available for IOP 3 and IOP 4. No radar data is available for IOP 6, and IOP 13 was a fairly dry case with strong waves and rotors but weak clouds. All these cases fall in a group of strong wave cases (Doyle et al. 2006; Smith et al. 2006) with intense low-level airflow perturbations, some of which appear quite different than the IOP 11 rotor.
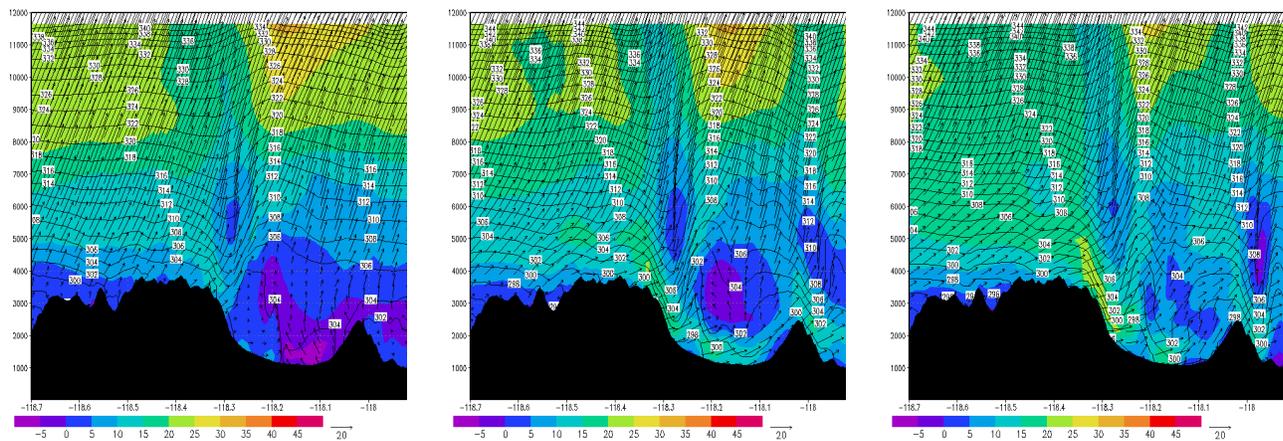
F_IG. 9: Vertical cross-sections of isentropes (K), E-W component of wind (m s$^{-1}$ in color) and horizontal wind (vectors) from the COAMPS simulation of IOP 11 for 0100 UTC April 10 (left), 0300 UTC April 10 (middle), and 0400 UTC April 10 (right). The base of these vertical cross-sections is parallel to the UWKA flight track. For explanation of the difference between the model output and observation times see text.

## REFERENCES

Baines, P. G., 1995: *Topographic Effects in Stratified Flows.* Cambridge University Press, 482 pp.

Batchelor, G. K., 1967: *An Introduction to Fluid Dynamics.* Cambridge University Press. 615 pp.

Damiani, R., and S. Haimov, 2006: A high-resolution dual-Doppler technique for fixed multi-antenna airborne radar, *IEEE Trans. Geosci. Remote Sensing.* In press.

Doyle, J. D., R. B. Smith, W. A. Cooper, V. Grubišić, J. Jensen, and Q. Jiang, 2006: Three-dimensional characteristics of mountain waves generated by the Sierra Nevada. *Online Proceedings.* $12^{th}$ *Conference on Mountain Meteorology.* Amer. Meteor. Soc. Paper **10.4**

Doyle, J. D., and D. R. Durran, 2002: The dynamics of mountain-wave induced rotors. *J. Atmos. Sci.*, **59**, 186–201.

Farmer, D., and L. Armi, 1999: Stratified flow over topography: The role of small scale entrainment and mixing in flow establishment. *Proc. Roy. Soc. Lond. A*, **455**, 3221–3258.

Grubišić, V., J. D. Doyle, J. Kuettner, G. S. Poulos, and C. D. Whiteman, 2004: Terrain-induced Rotor Experiment (T-REX) Overview Document and Experiment Design. 72 pp. Available at http://www.eol.ucar.edu/projects/trex/documents/.

Grubišić, V., and J. D. Doyle, 2006: Terrain-induced Rotor Experiment (Invited). *Online Proceedings.* $12^{th}$ *Conference on Mountain Meteorology.* Amer. Meteor. Soc. Paper **9.1**

Grubišić, V., and B. J. Billings, 2006: The intense lee-wave rotor event of Sierra Rotors IOP 8. *J. Atmos. Sci.*, Conditionally accepted.

Kuettner, J. P., 1959: The rotor flow in the lee of mountains. GRD Research Notes, No. 6, AFCRC–TN–58–626, ASTIA Document No. AD–208862, pp. 20.

Prandtl, L., 1952: *Essentials of Fluid Dynamics.* Hafner Publishing Company, 452 pp.

Smith, R. B., B. K. Woods, J. Jensen, W. A. Cooper, J. D. Doyle, Q. Jiang, V. Grubišić, 2006: Mountain effects entering the stratosphere: New aircraft data analysis techniques from T-REX. *Online Proceedings.* $12^{th}$ *Conference on Mountain Meteorology.* Amer. Meteor. Soc. Paper **10.5**